JOURNAL OF COMPUTATIONAL PHYSICS 94, 81–101 (1991)

Accuracy Analysis of a Bessel Spectral Function Method for the Solution of Scattering Equations

GEORGE H. RAWITSCHER

Physics Department, University of Connecticut, Storrs, Connecticut 06268

Received August 30, 1985; revised February 23, 1990

A Bessel function spectral method for obtaining the quantum-mechanical scattering wave functions, developed previously, was tested for the case that the potentials are complex Gaussian functions since, in this particular case, the required overlap integrals can be evaluated with great accuracy. The dependence of the elastic scattering S-matrix on the size of the space of the Bessel basis, on the choice of the sub-set of the basis functions, and on the choice of the matching radius was examined. The analysis is carried out to an accuracy of eight significant figures.

I. INTRODUCTION

Spectral methods for solving the Schrödinger equation for the case of bound state problems are well studied [1, 2]. If the functions to be approximated decrease exponentially, then it is known that the spectral expansion converges exponentially. However, in the case of scattering problems the properties of the spectral methods are less well understood because the scattering wave functions to be approximated are oscillatory and have amplitudes which asymptotically remain constant [2]. In this case one can include among the basis functions several which have the same asymptotic behavior (to within a constant to be determined) as the scattering function to be approximated [2]. A similar technique is used in the variational approaches to the scattering solutions [3, 4].

The present spectral method is being developed specifically to solve scattering problems [5]. In this method, which is of the Galerkin type, the spectral basis is composed of a discrete set of Bessel functions, each of which satisfies the appropriate physical scattering boundary condition. This is accomplished by introducing a sufficiently large radius R and, for each partial wave, matching the basis functions to the outgoing external wave function at R. This method will be denoted as the Sturmian spectral method (SSM) in what follows. Bessel functions rather than other functions such as polynomials are preferred, because for each partial wave they have the appropriate behavior of the exact scattering function, both at the origin and asymptotically. A study [6] of the Sturmian eigenfunctions of a scattering problem indeed showed that for the high partial waves, i.e., for angular momentum number L larger than 3 or 4, a Chebyshev expansion gave less accuracy

0021-9991/91 $3.00

than a Bessel expansion. Even though there are other methods for solving the quantum-mechanical scattering problem [3, 4, 7] which may be more efficient than the present one, it is the purpose of the present study to examine the numerical accuracy properties of the SSM in view of the usefulness of the SSM for special applications in physics.

One useful application of the SSM is in the calculation of effective scattering potentials [8–10]; another is in taking into account the Pauli exclusion principle in the interaction between two clusters of identical particles [11, 12]. The first application arises because the spectral representation of the wave-functions automatically leads to expressions for the many-channel Green's functions [8, 10]. This enables one to eliminate channels which one does not want to carry explicitly, thus giving rise to effective potentials in those channels which are kept. An example is the Feshbach optical model potential. It represents, in the elastic channel, the effect of all the virtual nuclear excitations which take place during the scattering process of a nucleon on a nucleus. A demonstration of the feasibility of calculating the Feshbach potential with this SSM has recently been given for a schematic coupled channel example [10], and further work along these lines is in progress [13].

The second application of the SSM, mentioned above, consists in the formulation of reaction theory for a system of indistinguishable particles. The difficulty here is in taking into account the Pauli exclusion principle. If all nucleons are bound, i.e., if all channels are closed, the conventional independent particle theory offers a suitable scheme. But when one or more nucleons are in the continuum, i.e., if one or more channels are open, then the corresponding extension of the independent particle formulation becomes very cumbersome [14]. In this case expansions into basis states other than the independent particle Shell-model states have been developed [15]. The expansion in terms of the Sturmian functions discussed here looks very promising in that only a very small set of basis functions (approximately six) is required in order to achieve good accuracy [11].

There are two basic types of Sturmian spectral functions. Those which asymptotically decrease exponentially [9, 16] (the negative energy case) and those which asymptotically oscillate like outgoing waves [17–19] (positive energy Sturmians). Both form a discrete set which is complete in the radial region where the eigenvalue potential which generates them is not zero [17]. As the size of the eigenvalue increases, the strength of the corresponding eigenvalue potential increases and the Sturmian functions acquire successively more nodes in the region of this potential. The present Sturmian functions [5] correspond to the positive energy category. A matching radius R is defined, and the eigenvalue potential is a square well in the radial interval from 0 to R. These functions, denoted as ϕ_i, in this case are proportional to spherical Bessel functions of complex wave number K_i. At the point R they are matched to outgoing wave Hankel functions of the asymptotic physical wave number k. In the interval $(0–R)$ the ϕ's are orthogonal. These functions are denoted as Bessel Sturmian functions, or BSF. More details are given in Section 3.

Positive energy Sturmians were first defined by Peierls in 1938, when they were used to develop R-matrix theory for the description of resonances in neutron–

nucleus scattering at low energies [18]. Negative energy Sturmians were first used intensively by Rotenberg in 1962 [16]. Subsequently, both positive and negative energy Sturmian functions have been used to construct separable representations of two-body scattering T-matrices [19] for the purpose of applying them to three-body calculations, and also for directly solving three-body problems [20].

In most of these applications not much attention has been paid to the question of accuracy. What makes the present accuracy study feasible is that the indefinite integrals, which are needed to set up the algebraic system of equations for the expansion coefficients, can now be calculated with high precision for the case that the potential is of the Gaussian form [21]. These integrals are obtained with a precision of better than 12 significant figures, and the scattering matrix element, which will be used as a measure for the accuracy tests, is calculated here with an accuracy of better than eight significant figures. In Section 2 the main equations which define the SSM will be presented; in Section 3 the accuracy tests will be described; and Section 4 contains the summary and conclusions.

II. Formalism

The coupled radial equations to be solved are

$$(T_L - E_n)\,\mathscr{F}_n(r) + \sum_{n'=1}^{N} V_{nn'}(r)\,\mathscr{F}_{n'}(r) = 0 \qquad (2.1)$$

$$n = 1, 2, \ldots, N,$$

where each channel is represented by the subscript n, E_n is the channel energy, the channel coupling potentials are $V_{n,n'}$, T_L is the partial wave kinetic energy operator $-(\hbar^2/2m)(d^2/dr^2 - L(L+1)/r^2)$, and $\mathscr{F}_n$ are the radial partial wave functions in each channel to be solved for. Asymptotically they are all outgoing waves, with the exception of the incident channel $n=1$, where $\mathscr{F}_1$ also has an admixture of an ingoing wave of unit amplitude. The physical channel wave numbers k_n are related to the channel energies E_n by $(\hbar^2/2m)\,k_n^2 = E_n$. The spherical regular and outgoing irregular Bessel functions are denoted by j_L and h_L, respectively, and f_L and g_L will be used to denote

$$f_L(z) = z j_L(z); \qquad g_L^{(+)} = z h_L(z). \qquad (2.2)$$

Here $g_L^{(+)}$ is asymptotically an outgoing function in z of the form $\exp(iz - iL\pi/2)$. The function $h_L(z)$ is equal to $ih_L^{(1)}(z)$, and both j_L and $h_L^{(1)}$ are defined in Abramowitz and Stegun [22].

The functions in each channel n which are needed for the calculation of the $\mathscr{F}$'s are of two types: the undistorted and uncoupled radial wave functions $F_n(r)$ which asymptotically have both ingoing and outgoing waves

$$F_n(r) = f_L(k_n r) \qquad (2.3)$$

and the set of Bessel Sturmian functions $\phi_{nj}(r)$, $j=1, 2, ...$, which asymptotically have only outgoing waves

$$\phi_{nj}(r) = \gamma_{nj} f_L(K_{nj} r), \qquad r < R \tag{2.4a}$$

$$\phi_{nj}(r) = \beta_{nj} g_L^{(+)}(k_n r), \qquad r \geqslant R. \tag{2.4b}$$

According to Eq. (2.4b), outside the boundary radius R all the BSFs for a given channel are proportional to the same outgoing wave function $g_L^{(+)}$. The normalization constants γ_{nj} in Eq. (2.4a) are obtained from the condition

$$\int_0^R \phi_{nj}(r)(T_L - E_n)\, \phi_{nj'}(r)\, dr = -\delta_{jj'}. \tag{2.5}$$

This integral can be carried out analytically, as is explained in Appendix A.

This set of definitions can be easily generalized to the case in which long-range potentials, such as the Coulomb potential, are present. For distances r larger than R the functions f and g are then replaced by regular and outgoing irregular Coulomb functions, but for $r < R$ the definition in terms of the spherical Bessel functions remains valid. This changes the value of the complex wave numbers K_{nj}, since the functions ϕ given by Eq. (4a) are now matched to outgoing Coulomb rather than Bessel functions. The functions $F_n(r)$ have to be renormalized for $r < R$, and they have to be matched to a combination of regular and irregular Coulomb functions at $r = R$. This generalization has been tested and it causes no special numerical difficulties. Other methods of including the long-range part of a distorting potential also exist [23]. In the present discussion, it will be assumed that no long-ranged potentials exist, such as the Coulomb potential, and all potentials (not including the centripetal potential) beyond the radial distance R will be assumed to vanish. This, however, means that the value of the matching radius R should be chosen large enough so that the neglect of the potentials $V_{nn'}$ beyond R is an acceptable approximation. This point is the subject of further discussion below.

The M-approximants to the solution of the coupled equations (2.1) are given by

$$\mathscr{F}_n^{(M)}(r) = \delta_{n1} F_1(r) + \sum_{j=1}^{M} c_{nj}^{(M)} \phi_{nj}(r). \tag{2.6}$$

The column vector $\mathbf{c}$ of the coefficients $c_{nj}^{(M)}$ are obtained from the matrix $\mathbf{V}$ and the column vector $\mathbf{b}$ by $\mathbf{c} = (\mathbf{I} - \mathbf{V})^{-1}\, \mathbf{b}$, where the column vectors are of length $M \times N$, and the matrices are of dimension $(M \times N)^2$. $\mathbf{I}$ is the identity matrix, and the elements of $\mathbf{V}$ and $\mathbf{b}$ are given by

$$V_{nj,n'j'} = \langle \phi_{nj} V_{nn'} \phi_{n'j'} \rangle \tag{2.7a}$$

and

$$b_{nj} = \langle \phi_{nj} V_{n1} F_1 \rangle. \tag{2.7b}$$

Here, and in what follows, the meaning of $\langle\ \rangle$ is the integral

$$\langle A \rangle = \int_0^R A(r)\, dr. \tag{2.8}$$

Thus, in Eqs. (7) the upper limit of the integration is R, and complex conjugation of the quantities ϕ_{nj} is not involved.

The scattering S-matrix elements are defined in terms of the asymptotic behavior of the functions $\mathscr{F}$,

$$\mathscr{F}_n(r) \approx [-g_L^{(-)}(k_n r)\, \delta_{n1} + S_{n1}\, g_L^{(+)}(k_n r)]/2i. \tag{2.9}$$

The function $g_L^{(+)}$ has been defined in Eq. (2), and $g_L^{(-)}$ is its complex conjugate. Defining the quantum-mechanical transition T-matrix from channels 1 to n as

$$T_{n1}(L) = \left\langle F_n \left(\sum_{n'=1}^{N} V_{nn'} \mathscr{F}_{n'} \right) \right\rangle, \tag{2.10}$$

one obtains the quantum-mechanical scattering matrix elements S for the transition from channel 1 to channel n:

$$S_{n1}(L) = \delta_{n1} - (4im/\hbar^2 k_n)\, T_{n1}(L). \tag{2.11}$$

In the case that long-range (Coulomb) potentials are also present it is sufficient to replace the functions $g_L^{(-)}$ and $g_L^{(+)}$ by the respective long-range distorted (Coulomb) ingoing and outgoing waves, and also to replace the δ in Eq. (2.11) by $S_n^{(0)}(L)\, \delta_{n1}$. Here $S_n^{(0)}(L)$ is the S-matrix element obtained when the function $f(k_n r)$ in channel n is matched to the combination of long-range distorted outgoing and ingoing (Coulomb) waves, in a manner defined by Eq. (2.9). The spectral Sturmian wave numbers K_{nj} are also changed since the Sturmian functions ϕ_{nj} are matched now to the long range distorted outgoing wave. This question will not be pursued further here.

Making use of Eq. (6), one obtains for the Mth approximant to T

$$T_{n1}^{(M)}(L) = \langle F_n V_{n1} F_1 \rangle + \sum_{j'=1}^{M} \sum_{n'=1}^{N} \langle F_n V_{nn'} \phi_{n'j'} \rangle\, c_{n'j'}^{(M)} \tag{2.12a}$$

with

$$c_{n'j'}^{(M)} = \sum_{j''=1}^{M} \sum_{n''=1}^{N} [\mathbf{I} - \mathbf{V}]^{-1}_{n'j',n''j''}\, b_{n''j''}. \tag{2.12b}$$

The above result, already given in Eq. (2.19) of Ref. [8] is the basic expression used for the numerical calculations. It can also be written as

$$T_{n1}^{(M)}(L) = \langle F_n V_{n1} F_1 \rangle + \sum_{j',j''=1}^{M} \sum_{n',n''=1}^{N} \times \langle F_n V_{nn'} \phi_{n'j'} \rangle [\mathbf{I} - \mathbf{V}]^{-1}_{n'j',n''j''} \langle \phi_{n''j''} V_{n''1} F_1 \rangle. \tag{2.12c}$$

According to this equation the quantum mechanical transition from state F_1 to state ϕ_{nj} takes place via the matrix element $\mathcal{O}_{n'',1}$,

$$\mathcal{O}_{n'',1}(K_{n''j''}, k_1) \equiv b_{n''j''} = \langle \phi_{n''j''} V_{n''1} F_1 \rangle. \tag{2.13}$$

It then "propagates" to the state $\Phi_{n'j'}$ via the distorted Green's function $[\mathbf{I} - \mathbf{V}]^{-1}_{n'j',n''j''}$ and finally ends up in state n via $\mathcal{O}_{n,n'}(k_n, K_{n'j'})$. The second-order Born approximation is obtained by replacing the propagator $[\mathbf{I} - \mathbf{V}]^{-1}$ by the unit matrix $\mathbf{I}$. In the next section numerical applications of the above formalism are described.

III. Numerical Accuracy Analysis for the Scattering Matrix Elements S

The two approximations made in the SSM described in Section II consist in assuming that the potentials V can be neglected for $r > R$, and in replacing the infinite space of the basis functions by a finite one. The latter occurs in the truncation of the sum over the j's in Eq. (2.6) or (2.12) at the upper limit M. One of the objectives of this section is to identify the part of the spectral basis which gives the major contribution to the sums in Eq. (2.12), especially when the incident energy is increased. Another objective is to examine the behavior of the S-value as a function of the choice of the matching radius R.

The numerical example consists of a neutron incident at energies between 15 and 240 MeV on a nucleus approximately of the size of ^{16}O. All the potentials $V_{nn'}$ in Eq. (2.1) are of the Gaussian form

$$V(r) = (V_0 + iW_0) \exp[-(r/a)^2], \tag{3.1}$$

where the parameters V_0, W_0 and a are given specific values for each combination of n and n'. For this Gaussian case the indefinite integrals (2.7), which are needed for the elements of the matrix $\mathbf{V}$ and of the vector $\mathbf{b}$, are calculated with an accuracy to better than 10 significant figures by the recursion-relation method described in Ref. [21]. With these results, and for a given choice of the upper limit of summation M, the coefficients $\mathbf{c}^{(M)}$ are obtained from Eq. (2.12b) by using the linear equations subroutine LEQ2C from the International Mathematical and Statistical Libraries (IMSL) subroutine package. The spectral wave-numbers K_{nj} needed for the specification of the spectral BSFs are obtained numerically to better than eight

significant figures by a complex Newton–Cotes iterative procedure, which is described in the Appendix of Ref. [6]. The logarithmic derivatives at the matching radius R needed for the calculation of the wave numbers K_{nj} are obtained from the regular and irregular functions $f_L(k_n R)$ and $g_L(k_n R)$ and their derivatives, which are defined in Eq. (2.2). The latter are read into the program with eight significant figures. All calculations are done in double precision on an IBM 3081 computer.

The scattering S-matrix elements are obtained from Eqs. (2.11) and (2.12). Because of the truncation of the sums over the indices j at the upper limit M, the result for the elastic scattering matrix element is denoted as $S^{(M)}$. The maximum value of M is denoted as MAX. The numerical value of $S^{(\mathrm{MAX})}$ was compared with

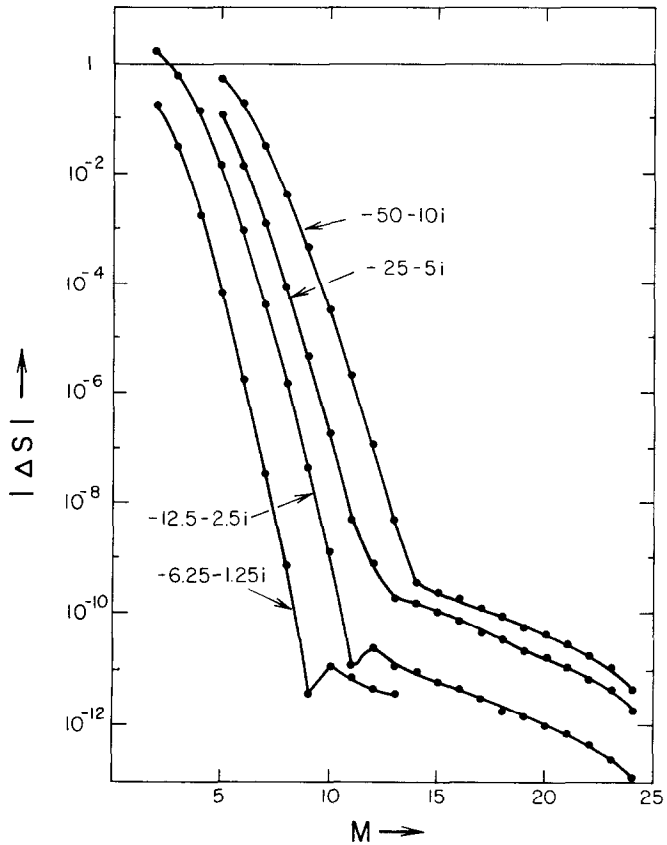

FIG. 1. Convergence of the elastic S-matrix elements $S^{(M)}$ with the size M of the SBF basis for various strengths of the distorting Gaussian potentials. The quantity $|\Delta S|$ is the absolute value of $S^{(M)}$-$S^{(25)}$. The angular momentum L is zero; the matching radius $R = 11$ fm and the example corresponds to elastic neutron–oxygen scattering at an incident energy of 15 MeV. The distorting potential is of Gaussian form given by Eq. (3.1). The value of the diffuseness **a** is 4 fm, the values of the depths $V_0 + iW_0$ are indicated by the numbers next to the curves, in units of MeV. The maximum value of M is MAX = 25.

the result obtained from a conventional marching algorithm (Milne's method given by Eq. (25.5.21C) of Ref. [22]), both for a single channel and a coupled channel case, and good agreement was found to better than four significant figures. However, the accuracy of the marching method was not analyzed to the same number of digits as the SSM, and thus the "exact" value of S is unknown. For the present purpose the exact value of S is replaced by $S^{(\mathrm{MAX})}$, where the value of MAX is chosen as described below. A measure of the rapidity of the convergence of $S^{(M)}$ is obtained by calculating the absolute value of the difference between $S^{(\mathrm{M})}$ and $S^{(\mathrm{MAX})}$

$$\Delta S(M) = |S^{(M)} - S^{(\mathrm{MAX})}|. \tag{3.2}$$

3.1. *Convergence of S with the Size M of the BSF Basis*

In this subsection the sums over j and j' in Eq. (2.12) are carried sequentially from 1 to the upper limit M, and the dependence of the corresponding scattering matrix element $S^{(M)}$ with M will be examined.

The results for ΔS for an uncoupled case (i.e., $N=1$) are illustrated in Fig. 1. A neutron with laboratory energy of 15 MeV is incident on a nucleus with mass number 16. The potential V_{11} is given by Eq. (1) with the value of the surface diffuseness $a=4$ fm, and various sets of potential strengths (V_0, W_0), which decrease successively by factors of two, are used to test the rate of convergence of S with M as a function of the potential strength. The largest values of (V_0, W_0) are $(-50$ MeV, -10 MeV), which is a reasonable value for the optical potentials which occur in the description of nucleon–nucleus scattering. The value of MAX is 25, the matching radius is chosen to have the value of 11 fm.

The following features emerge from Fig. 1:

(a) The error in $S^{(M)}$ decreases nearly exponentially with M for $M>5$. For each successive value of M the error decreases roughly by one order of magnitude. This fast decrease comes to an abrupt halt at a particular value of M, denoted as M_c, where the speed of the convergence decreases.

(b) The smaller the value of $V+iW$, the more rapidly a given accuracy for the S-matrix elements can be achieved.

For spectral methods an exponential convergence with M is expected for the expansion of functions which have no special singularities, such as the scattering functions $\mathscr{F}$ whose expansion is given in Eq. (2.6). The increase of accuracy with a decrease of the potential strength is to be expected, since the smaller the potential, the less the distorted wave function ($\mathscr{F}$) differs from the undistorted one (F), and hence fewer terms are needed in the sum in Eq. (2.6). For a given value of M (for example, $M=9$) the accuracy of S increases by two orders of magnitude every time the strength of the potential is decreased by a factor of two. This observation shows that the SSM is much more powerful than second-order perturbation theory, for

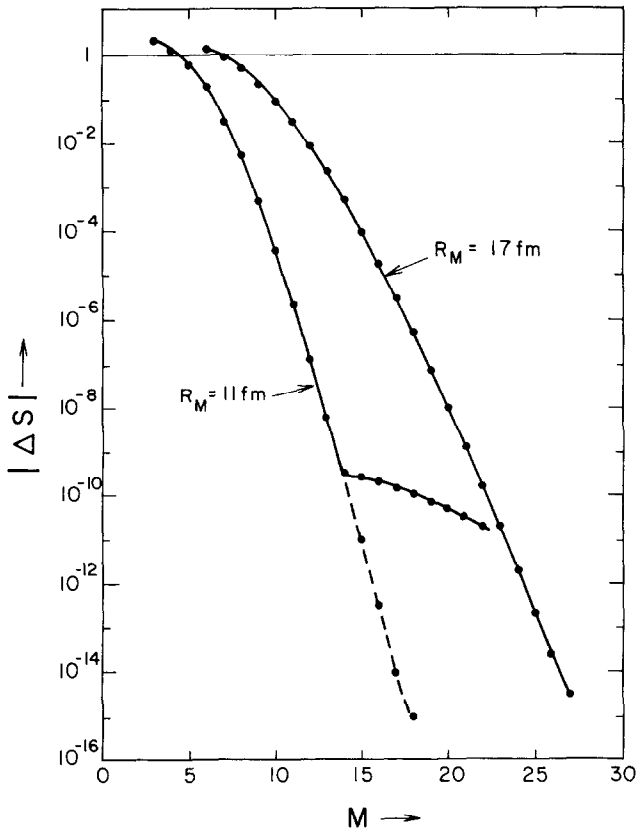

FIG. 2. Same as Fig. 1 for two different values of R, indicated in the figure. The solid (dashed) lines indicate the results obtained with method $F(I)$ in which the upper limit of all integrals in Eqs. (2.7) is equal to $R(\infty)$. The maximum value of M is MAX = 30.

which the accuracy is expected to increase with the square of the reduction factor of the potential.

The change in slope at M_c is due to the non-vanishing value of the potential at R, as will be now be demonstrated. When the value of the potential at R is decreased, which can be accomplished by either decreasing the diffuseness a of the Gaussian, or by increasing the value of R, or by decreasing the value $V_0 + iW_0$, then the position of the break is shifted to smaller values of ΔS. This is illustrated in Fig. 2, where the value of R is increased from 11 to 17 fm, with (V, W, a) being kept constant at their values $(-50$ MeV, -10 MeV, 4 fm). The corresponding ratio of $V(r=R)/V(r=0)$ is thereby decreased from 5.2×10^{-4} to 1.4×10^{-8}. Up to an accuracy of 10^{-13} no break occurs in the slope of the curve for $R=17$, while for $R=11$ the break occurs in the vicinity of 10^{-9}. If one replaces the integrals calculated from $r=0$ to $r=R$ in Eqs. (2.7) by the corresponding integrals from $r=0$ to $R=\infty$, one obtains the results indicated by the dashed line in Fig. 2. For

TABLE I

S-Matrix Elements for Two Different Values of R^a

R (fm)	Re(S)	Im(S)	Method^b	$\cdots$	$\lvert\Delta S\rvert^c$
11	0.208046555	0.250191842	*F*		1.46 [−4]
17	0.207991512	0.250056867	*F*		1.42 [−8]
11	0.207989274	0.250056637	*I*		2.24 [−6]
17	0.207991501	0.250056876	*I*		—

[a] The incident lab energy is 15 MeV, (V, W, a) have the values (−50 MeV, −10 MeV, 4 fm), there is only one channel, the value of the angular momentum is $L=0$.

[b] In method *F* the radial integrals in Eqs. (2.7) go from $r=0$ to $r=R$. In method *I* the same integrals go from 0 to ∞.

[c] $|\Delta S|$ denotes the absolute value of the difference between the value of S in the table and the value of S given for $R=17$ fm, method *I*.

$R=17$ fm the results for ΔS for the two methods of calculation are nearly identical up to the values shown, and for $R=11$ fm they differ significantly only beyond the value of M where the change in slope occurs.

The two methods of calculation using either the finite or the infinite value of the upper limit of the integration are denoted as methods *F* and *I*, respectively. The values of the S matrix elements obtained for the two methods are given in Table I. The error in S relative to the most accurate value is denoted as $|\Delta S|$ in Table I. It is interesting to note that using method I instead of *F* at $R=11$ fm reduces the error in S by a factor of 65. This result probably can be shown to follow from the particular variational principle upon which the SSM is based [3, 4, 24], but a proof is beyond the scope of this investigation. That the slope of the curve of $|\Delta S|$ with M is less steep for the larger value of R can be understood from the fact that there are fewer oscillations per unit length in the basis functions ϕ_{nj} for a given value of j the larger the value of R, and hence the overlap integrals $b_j=\langle\Phi_j V F_0\rangle$ which "drive" the coefficients c_j, decrease more slowly with j also. The absolute values of these overlap integrals are displayed in Fig. 3 in order to illustrate the above remark, and also in order to show the effect of cutting the integration off at $r=R$. The dashed lines show the result for the integral when the upper limit is equal to ∞. These values are very close to the result obtained with the upper limit equal to R (solid lines) for the small values of j because the contribution to the integral from the radial region beyond R is negligible compared to the total integral. As j increases, the contribution to the integral from the tail region beyond R becomes comparable to the contribution from the interval $0<r<R$, and methods *I* and *F* give very different results.

The above results also hold for the case of channel coupling, with the exception that for the *S*-matrix element in the elastic channel it is not as critical that the

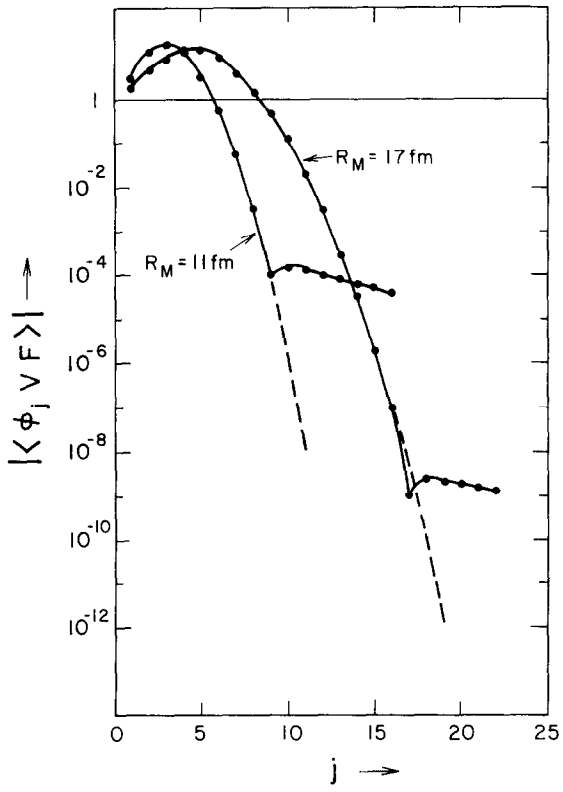

FIG. 3. The absolute value of the overlap integrals $\langle \phi_j V F_0 \rangle$ in units of $(\text{MeV fm})^{1/2}$ for two values of R for the case described in Fig. 1. The notation and the value of MAX is he same as in Fig. 2.

potentials in the inelastic channels be small at the position of the matching radius. What has to be small are the coupling potentials V_{1n} between the incident channel and the other channels at R. This is illustrated in Fig. 4. In this case a Coulomb potential is present, and the figure shows the elastic S-matrix element for the scattering of 21.6 MeV deuterons on the nucleus of ^{64}Ni for an angular momentum $L = 0$. The maximum number of channels employed is six; the excitation energies in channels 1, 2, ..., 6 are 0, 2.923, 4.888, 8.008, 12.245, and 17.592 MeV, respectively. The matching radius is at 12 fm. In the radial region $0 < r < 12$ fm only Gaussian potentials of the form of Eq. (3.1) are assumed. The values of the parameters V_0, W_0 and a are given in Table II. The corresponding values of ΔS are shown in Fig. 4 by the curves labeled "*A*." The accuracy for the one-channel case is much higher than for the two- or six-channel cases because the coupling potential V_{12} was chosen to have a long range ($\mathbf{a} = 7$ fm) so that its value at R is not small. When the range of V_{12} is reduced to $\mathbf{a} = 5$ fm, then the accuracy improves, as is illustrated by the curves marked "*B*."

Similar results apply for angular momenta $L \neq 0$. Since the angular momentum barrier shields the Gaussian potentials at small distances, the distorting potentials

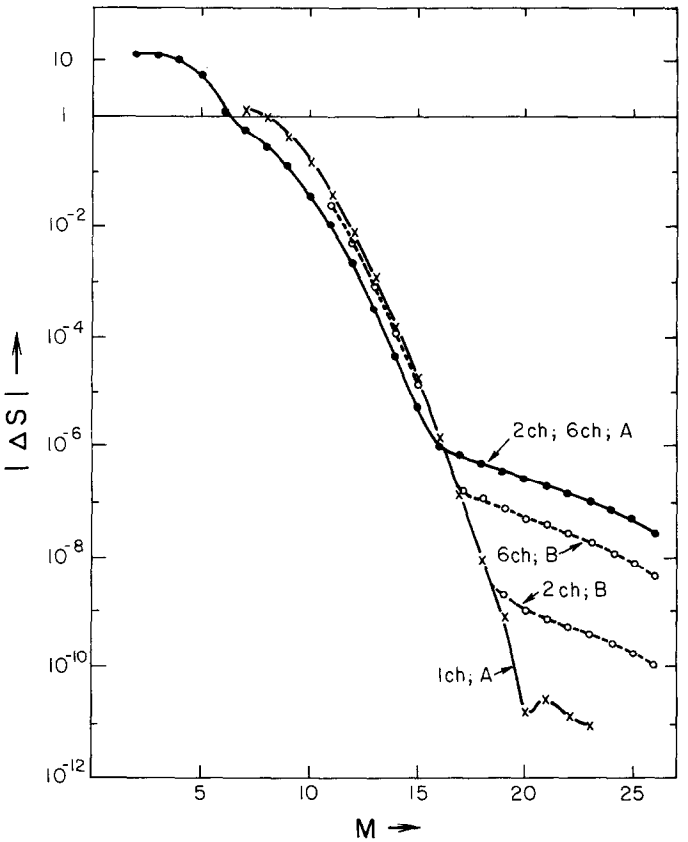

FIG. 4. Convergence of $S^{(M)}$ with M for various coupled channel cases, described in the text. It illustrates that the size of the inelastic inter-channel coupling potentials at R is not as important for the accuracy as is the size of the elastic to inelastic coupling potentials.

are effectively smaller and good accuracy is already achieved for a smaller size M of the Sturmian space. However, the change in slope of the plot of ΔS with M also occurs, and sets in at a value of M_e which is close to that for the $L=0$ case.

In conclusion, if a good accuracy in the S-matrix element is desired then the choice of the matching radius should be such that the distorting potentials are sufficiently small beyond R. However, the larger R, the more basis functions are required. If long range potentials are present in the diagonal potentials, such as Coulomb potentials, for example, it is preferable to include their effect in the outgoing radial functions to which the Bessel–Sturmian functions are matched. If, however, long-range potentials are also present in the coupling potentials, then a different procedure to handle this case may be required.

3.2. *Selection of the Relevant Space of the BSF Basis*

As the energy increases, the upper limit M of the *BSF* basis increases correspondingly; however, not all the basis functions $j=1, 2, ..., M$ contribute equally

TABLE II

Gaussian Potential parameters, Defined in Eq. (3.1), for the Channel Potentials $V_{nn'}(r)$, case A, used in the calculation for Fig. 4

Channel					Channel				
		V	W	a			V	W	a
n	n'	(MeV)	(MeV)	(fm)	n	n'	(MeV)	(MeV)	(fm)
1	1	−50	−10	4	5	1	−4	−2	4
2	1	−11	−4	7	5	2	−10	−3	10
2	2	−10	−5	7	5	3	−30	−5	10
3	1	−8	−2	4	5	4	−35	−6	10
3	2	−15	−4	10	5	5	−40	−7	6
3	3	−2.5	−6	6	6	1	−2	−2	4
4	1	−6	−2	4	6	2	−8	−3	10
4	2	−12	−3.3	10	6	3	−35	−4	10
4	3	−20	−4	10	6	4	−40	−4	10
4	4	−30	−7	6	6	5	−45	−5	10
					6	6	−45	−10	7

to the expansion. Identifying which basis functions are the important ones is the subject of this sub-section.

Figure 5 shows the dependence of ΔS with M for various energies for the same n-^{16}O example which is discussed in Section 3.1 above. In this calculation there is only one channel, the potential parameters (V_0, W_0, a) are again given by $(-50\text{ MeV}, -10\text{ MeV}, 4\text{ fm})$ and the value of R is 11 fm. It is seen that, as the incident energy increases, the upper limit M of the BSF basis also increases, but the slope of the curve of ΔS with M is the same for all energies. The main difference between the various cases is that the various curves are shifted to the right relative to each other. The value of M beyond which ΔS starts to decrease with M is denoted as M_0 in what follows.

The increase of M_0 with energy can be understood in terms of the behavior of the overlap integrals $\mathcal{O}$, defined in Eq. (2.13), as will now be discussed. Absolute values of $\mathcal{O}_{n,1}(K_{nj}, k_1)$ are illustrated in Fig. 6 by the bell-shaped curves for a two-channel 240 MeV n-^{16}O example. They are labeled as $\mathcal{O}_n$ in the figure. The potential parameters are listed in Table III. It can be seen that the maximum of $\mathcal{O}_{n1}$ occurs for a value of j, to be denoted as j_M, such that the real part of K_j is closest to the incident channel wave number k. This is confirmed in Table IV, wich lists values of K_{1j} and k_1 for various incident neutron energies and orbital angular momenta L. For 240 MeV, K_j is close to k for j between 11 and 12 for $L=0$, and, indeed, in Fig. 6 this is where the maximum of $\mathcal{O}_1$ occurs. Beyond this value of j, ΔS begins to decrease with M (shown by the full circles), which is consistent with the decrease of the $\mathcal{O}$'s with j.

For values of j progressively less than j_M the contribution to S of the basis states is also correspondingly small. This can be demonstrated by eliminating all basis

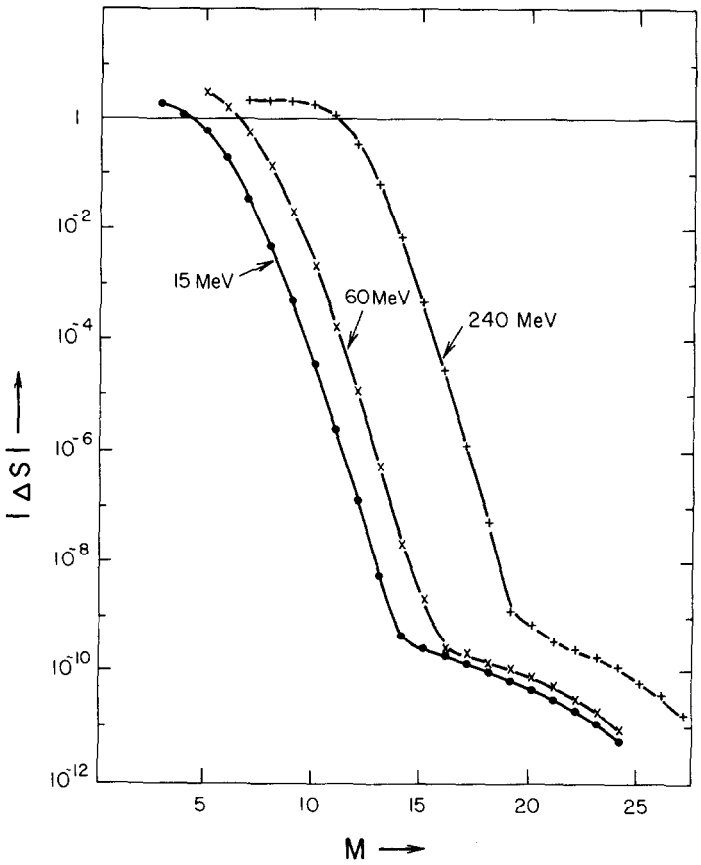

FIG. 5. Convergence of $S^{(M)}$ with M as a function of incident projectile energy. The calculation is for the case described in Fig. 1. One channel only is included, the Gaussian potential has a depth of $-50 - 10i$ MeV, the diffuseness is $a = 4$ fm, the matching radius $R = 11$ fm.

TABLE III

Same as Table II for the Calculation Illustrated in Fig. 6

Channel		V	W	a
n	n'	(MeV)	(MeV)	(fm)
1	1	−50	−10	4
2	1	−11	−4	5
2	2	−10	−5	7

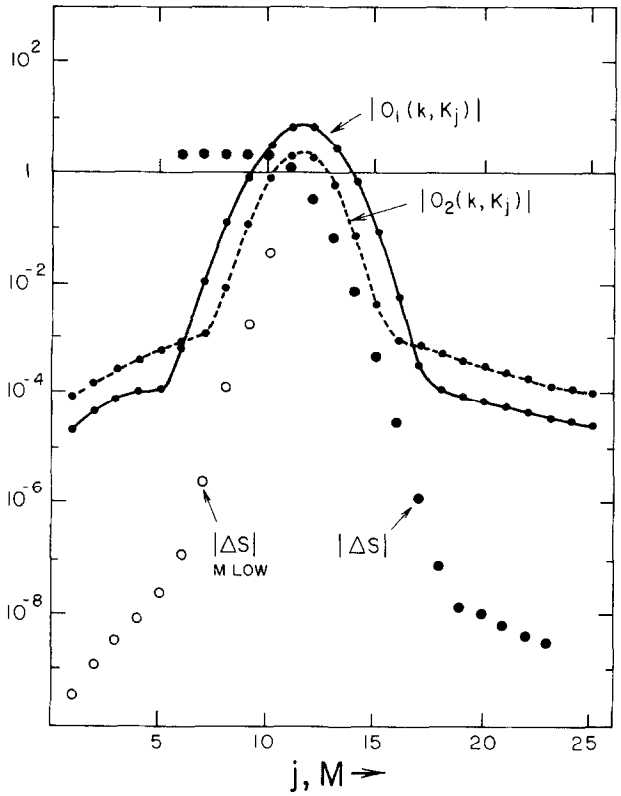

FIG. 6. How to choose the important basis functions. The large solid and open circles illustrate values of $|\Delta S^{(M)}|$. The solid circles give the results obtained when the SBF's ϕ_{nj} included in the calculation have values of j which run from 1 to M. The open circles illustrate the values of $|\Delta S^{(M)}|$ when the values of j start at MLOW and run to MAX = 25, with MLOW increasing progressively from 1 to a maximum value of 10. Thus, when the values of j run from 8 to 16, one achieves an accuracy in S of one part in 10^4. This example corresponds to a two-channel calculation for 240 MeV neutrons incident on ^{16}O. The gaussian potentials are listed in Table III. The orbital angular momentum $L = 0$, and the matching radius is $R = 11$ fm. The bell-shaped curves illustrate overlap matrix integrals O_{n1}, defined in Eq. (2.13), as a function of the Sturmian index j, in units of (MeV fm)$^{1/2}$. The peaks occur when K_j is close to the channel momentum k, as can be seen from Table IV.

states ϕ_{nj} for $j = 1, 2, ...,$ MLOW from the calculations of the matrix **V** and from the column vector **b**, and carrying out the sums in Eq. (2.12) from $j =$ MLOW to $j =$ MAX. The result for ΔS is indicated by the open circles in Fig. 6, where in the abscissa M stands for MLOW. By combining the information from the open and closed circles, one can deduce that an accuracy of better than five figures for S can be obtained if a band of 11 j-values, from $j = 7$ to $j = 17$ is used in the evaluation of Eq. (2.12). This band straddles the K_j values around $K_j \cong k$ at the center.

In conclusion, it is shown that the important basis functions are the ones whose number of nodes in a given radial interval is comparable to the number of nodes

TABLE IV

Wave Number K_j for n-0^{16} Scattering, in Units of fm^{-1}

E_L(MeV)	15	240	15	240
$k(fm^{-1})$	0.797	3.189	0.797	3.189
R(fm)	11	11	20	11 $L=5$
j	K_j	K_j	K_j	K_j
1	0.281	0.285	0.156	0.850
2	0.555	0.571	0.313	1.178
3	0.786	0.856	0.468	1.485
4	1.016	1.141	0.620	1.784
5	1.290	1.426	0.757	2.079
6	1.573	1.711	0.880	2.370
7	1.857	1.996	1.026	2.656
8	2.143	2.280	1.180	2.933
9	2.428	2.562	1.336	3.176
10	2.713	2.839	1.493	3.416
11	2.999	3.094	1.650	3.689
12	3.284	3.323	1.807	3.972

[a] K_j are the Sturmian–Bessel wave numbers defined in Eq. (2.4). Only the real parts, in units of fm^{-1}, are listed. The physical wave number is denoted by k. It is related to the energy by $E=(\hbar k)^2/2m$. The orbital angular momentum L for the first three columns is 0. For the last column it is 5.

of the incident wave, at least for the Gaussian potentials studied in this paper. This type of behaviour has been found also to hold in the spectral solution of the Mathieu equation [2], where it is called "sideband truncation" of the basis set.

IV. Summary and Conclusions

In view of the increased usefulness for certain applications in physics of the spec-

as a result of the advent of a very accurate method to evaluate the required Bessel function overlap integrals [21], a study of the accuracy of the Bessel–Sturmian (BSF) expansion method (SSM) for calculating elastic scattering S-matrix elements was carried out. The diagonal as well as the coupling potentials used in the Schrödinger equation were of Gaussian form, with magnitudes of the type encountered in nuclear physics applications. It was found that the error decreased exponentially with the number of basis functions included in the calculation, but the accuracy does not increase beyond a certain value as a result of the cutoff of the potential at the matching radius R. The smaller the value of the potential at R, the better the final accuracy which is achieved. Accuracies typically of the order of one part in 10^7 could be achieved with about 15 BSF elements in each channel.

In detail, the conclusions reached from the experience with the gaussian potentials are:

(a) In order to obtain good accuracy for S the diagonal potential in the elastic channel, as well as the coupling potentials between the elastic and inelastic channels should be small beyond the matching radius R. The choice of R is thus governed by the range of the potentials. However, the larger the R, the more basis functions are required. If long-range potentials are present in the diagonal potentials, such as Coulomb potentials, for example, it is preferable to include their effect in the outgoing radial functions to which the Bessel–Sturmian functions are matched. If long-range potentials are also present in the coupling potentials, then a different procedure to handle this case may be required.

(b) The important basis functions which are needed to obtain good accuracy are the ones for which the overlap matrix elements $\mathcal{C}_{n1}$ (of the potential taken between the incident wave and the basis functions in channel n) are large. For a smooth potential, such as of the Gaussian form discussed here, this is the case when the number of nodes of the basis functions in the interval 0–R is comparable to that of the incident wave. However, if the potentials have strong repulsive cores, so as to have large Fourier components for a large range of Fourier momenta, then the above condition is no longer applicable. This was found to be the case in a study of the representation of the scattering T-matrix for nucleon–nucleon potentials of the Reid soft core variety [25].

(c) The requirement in (a) that the potential be small beyond the matching radius R can be softened by replacing the upper limit R of the integrals by infinity. An improvement by a factor of 65 in the accuracy in a sample case listed in Table I could thereby be achieved. An explanation based on the variational method which underlies the SSM has not yet been carried out.

(d) The computation time for the SSM method could become competitive with the more conventional radial mesh "marching" algorithms when the number of channels (N) becomes large and when the incident energy increases. For the present application to Gaussian potentials, for which analytical methods for calculating the overlap integrals exist, an estimate based on Table V in Appendix B shows that the crossover point occurs at 80 channels. However, this result is very strongly dependent on the type of the method of solution used [7], as well as on the architecture of the computer employed. For example, since most of the computation time is spent on obtaining the matrix elements of **V** (their number is proportional to N^2), which can be calculated independently from each other, a computer with parallel architecture probably will favor the SSM already for a smaller number of channels.

Appendix A: Normalization of the Spectral Bessel Functions

An analytical expression will now be given for the normalization constants γ_{nj} of the BSFs defined in Eq. (2.4), such that the normalization integral (2.5) is satisfied.

The result is

$$\gamma_{nj}^{-1} = f_L(z_{nj})\{\bar{V}_{nj} R[z_{nj}^2 + B_n^2 - B_n + L^2 - L]/(2z_{nj}^2)\}^{1/2}. \tag{A.1}$$

Here

$$z_{nj} = RK_{nj} \tag{A.2}$$

and

$$\bar{V}_{nj} = E_n - (\hbar K_{nj})^2/2m \tag{A.3}$$

is the complex square well potential depth for which $f_L(z_{nj})$ is the corresponding solution of the radial Schrödinger equation. The depth is determined such that F_L smoothly matches the solution given by Eq. (2.4b) for $r \geqslant R$. The constants B_n represent the logarithmic derivatives

$$B_n = \{[r\, dH_{CL}^{(+)}(k_n r)/dr]/H_{CL}^{(+)}(k_n r)\}_{r=R}. \tag{A.4}$$

The result (A.1) follows from the analytical and recursion relation properties of Bessel functions. One can convince oneself that the imaginary part of the quantity in square brackets in Eq. (A.1) is negative and never zero.

Appendix B: Computation Time

The computation times for the various steps needed in the calculation are listed in Table V. These times are obtained in $\frac{1}{100}$th of a second from a time-measuring subroutine inserted in various points in the Fortran program during execution time. The calculation is done on an IBM 3081 model K in double precision, but is not vectorized. The time measurements are only accurate to about 10%, since repetition of a run would not exactly reproduce the previous one. The entry labeled "Total" was extracted from the CPU time for the final Go step.

Table V shows that by far the largest block of time is used for the calculation of the overlap integrals (2.7) needed for the elements of the matrix **V**. Since, for a given value M of the Sturmian basis, the number of such elements is roughly proportional to N^2, one expects that the total computing time is also proportional to N^2 for large N. This is indeed borne out by the line in this table labeled Total/N^2. By contrast, the conventional marching algorithm method of solving the coupled equations (Milne's method given by Eq. (25.5.21 C) of Ref. [22]) increases considerably faster than N^2. Even though for six channels the conventional method is still 12 times faster than the SSM described in this paper, an extrapolation based on this table shows that for a number of channels larger than 80, the SSM method will be faster. Further, as is shown in Section 3.2, the number of basis functions

TABLE V

Computation Time in $\frac{1}{100}$th of a Second for Various Parts of the SSM Calculation, as Measured on a IBM 3081 Scalar Processor

N^a	1	2	4	6
$F_1{}^b$	8	1	2	1
$K_{nj}{}^c$	17	32	62	93
$\mathbf{V}^d$	145	374	111	2534
Lin. Eq.^{e}	10	44	197	482
Total SSM^f	213	569	1877	4351
$\mathbf{V}/N^2$	145	94	69	70
Lin. Eq./N^2	10	11	12	13
Total SSM/N^2	213	142	117	120
$(\mathrm{SSM}/MA)_{\mathrm{Total}}{}^g$	39	23	15.5	12

Note. The number of Sturmian states is $M = 18$, the orbital angular momentum $L = 10$.

[a] N is the number of channels in the coupled equations.

[b] Calculation of various constants associated to F_1 defined in Eq. (2.3).

[c] Calculation of the Sturmian quantities K_{nj} and γ_{nj} defined in Eq. (2.4).

[d] Calculation of the matrix elements (2.7) by the method of Ref. [21].

[e] Solution of the linear equations (2.12b) for the coefficients $c_{nj}^{(M)}$.

[f] Because of several other steps in the calculation, this number exceeds the sum of the various components listed above.

[g] This entry is the ratio of the total calculation time for the SSM as compared to the conventional method *MA*. The latter is Milne's marching algorithm [22] for solving the coupled equations. It uses a radial mesh with 384 points in each channel.

needed is independent of the incident energy. Hence, the computational effort of the SSM is also independent of the incident energy if analytic expressions for the matrix elements of **V** exist. This is not the case for the marching algorithm, since the radial mesh size has to be reduced as the energy increases, so as not to loose accuracy.

ACKNOWLEDGMENTS

This work was supported by NSF Grants PHY-8317440 and PHY-8901624. Conversations with Professor Y. Hahn concerning the variational aspects of the SSM were very helpful. A critical reading of the manuscript by Dr. George Delic is much appreciated. The availability of the excellent facilities of the University of Connecticut Computer Center is also of great value.

REFERENCES

1. D. GOTTLIEB AND S. A. ORZAG, *Numerical Analysis of Spectral Methods: Theory and Applications* (SIAM-CBMS, Philadelphia, 1977); C. CANUTO, M. Y. HUSSANI, A. QUARTERONI, AND T. A. ZANG, *Spectral Methods in Fluid Dynamics*, Springer Series in Computational Physics (Springer-Verlag, New York, 1988).
2. J. P. BOYD, *Chebyshev and Fourier Spectral Methods*, Lecture Notes in Engineering, Vol. 49, Springer-Verlag, New York, 1989); J. P. BOYD, *Comput. Phys.* **4**, 83 (1990).
3. R. G. NEWTON, *Scattering Theory of Waves and Particles* (McGraw-Hill, New York, 1966), 1st, p. 319; B. H. BRANDEN, *Atomic Collision Theory* (Benjamin, New York, 1970), Chap. 2, 5; Y. HAHN, *Phys. Rev. A* **32**, 2496 (1985).
4. W. SCHWENKE, K. HAUG, M. ZHAO, D. G. TRUHLAR, Y. SUN, J. Z. H. ZHANG, AND D. J. KOURI, *J. Phys. Chem.* **92**, 3202 (1988); Y. SUN, D. J. KOURI, AND D. G. TRUHLAR, *Nucl. Phys. A* **508**, C41 (1990).
5. G. H. RAWITSCHER, *Phys. Rev. C* **25**, 2196 (1982); G. H. RAWITSCHER AND G. DELIC, *Phys. Rev. C* **29**, 747 (1984); G. DELIC AND G. H. RAWITSCHER, *J. Comput. Phys.* **57**, 188 (1985).
6. G. H. RAWITSCHER AND G. DELIC, *J. Math. Phys.* **27**, 816 (1986).
7. D. SECREST AND B. R. JOHNSON, *J. Chem. Phys.* **45**, 4556 (1966); B. R. JOHNSON AND D. SECREST, *J. Chem. Phys.* **48**, 4682 (1968); R. G. GORDON, *J. Chem. Phys.* **51**, 14 (1969); W. N. SAMS AND D. J. KOURI, *J. Chem. Phys.* **51**, 4809, 4815 (1969); J. C. LIGHT AND R. B. WALKER, *J. Chem. Phys.* **65**, 4272 (1976); G. A. PARKER, T. G. SCHMALZ, AND J. C. LIGHT, *J. Chem. Phys.* **73**, 1757 (1980); F. MRUGALA, *J. Comput. Phys.* **58**, 113 (1985).
8. G. H. RAWITSCHER AND G. DELIC, *Phys. Rev. C* **29**, 747 (1984).
9. L. CANTON AND G. PISENT, *Acta Phys. Austr. Suppl.* **27**, 645 (1985); L. CANTON AND G. PISENT, In *Proceedings*, "*Primo covegno su problemi di fisica nucleare teorica*," edited by L. Bracci *et al.* (1985), p. 75; G. CATTAPAN, L. CANTON, AND G. PISENT, *Proceedings Few-Body Conference XII, Vancouver 1989*," edited by B. K. JENNINGS.
10. G. H. RAWITSCHER, *Nucl. Phys. A* **475**, 519 (1987).
11. M. BUBALLA, A. GATTONE, R. DE HARO, R. JESSENBERGER, AND S. KREWALD, *Nucl. Phys. A* **517**, 61 (1990).
12. G. H. RAWITSCHER, "Optical Potential with Two-Nucleon Correlations," Symposium on the occasion of the 40th Anniversary of the Nuclear Shell Model, Argonne National Laboratory, Argonne, IL, May 25, 1989.
13. G. CATTAPAN, L. CANTON, AND G. PISENT, *Phys. Lett. B* **240**, 1 (1990).
14. C. MAHAUX AND H. A. WEIDENMÜLLER *Shell-Model Approach to Nuclear Reactions* (Americal Elsevier, New York, 1969); D. EPPEL AND A. LINDNER, *Nucl. Phys. A* **240**, 437 (1975); W.-M. WENDLER, *Nucl. Phys. A* **472**, 26 (1987).
15. R. J. PHILPOTT, *Phys. Rev. C* **7**, 869 (1973); D. HALDERSON AND R. J. PHILPOTT, *Nucl. Phys. A* **345**, 141 (1980).
16. M. [illegible] *Phys.* (N.Y.) **19**, 262 (1962); M. [illegible] *Nucl. Phys. A* **116**, 83 (1968); (1964); R. G. Newton, *Scattering Theory of Waves and Particles* (McGraw-Hill, New York, 1966), pp. 198, 282.
18. P. L. KAPUR AND R. E. PEIERLS, *Proc. Roy. Soc. (London) A* **166**, 277 (1938); R. E. PEIERLS, *Proc. Cambridge Phil. Soc.* **44**, 242 (1948).
19. J. S. BALL AND D. Y. WONG, *Phys. Rev.* **169**, 1362 (1968); M. G. FUDA, *Phys. Rev.* **186**, 1078 (1969). T. BRADY, M. FUDA, E. HARMS, J. S. LEVINGER, AND R. STAGAT, *Phys. Rev.* **186**, 1069 (1969); J. S. LEVINGER, A. H. LU, AND R. STAGAT, *Phys. Rev.* **179**, 926 (1969); A. G. SITENKO AND V. F. KHARCHENKO, *Sov. Phys. Uspekhi* **14**, 125 (1971); A. G. SITENKO, V. F. KHARCHENKO, AND N. M. PETROV, *Phys. Lett. B* **28**, 308 (1968); K. HARTT AND P. V. A. YIDANA, *Phys. Rev. C* **36**, 475 (1987); G. PISENT AND L. CANTON, *Nuovo Cim. A* **91**, 33 (1986); L. CANTON, G. CATTAPAN, AND

G. PISENT, *Nuovo Cim. A* **97**, 319 (1987); L. CANTON, G. CATTAPAN, AND G. PISENT, *Nucl. Phys. A* **487**, 333 (1988); A. C. FONSECA, *Lecture Notes in Physics*, Vol. 273 (Springer-Verlag, Berlin, 1987).

20. S. A. SOFIANOS, H. FIEDELDEY, H. HABERZETTL, AND W. SANDHAS, *Phys. Rev. C* **26**, 228 (1982); E. O. ALT AND W. SANDHAS, *Phys. Rev. C* **18**, 1088 (1979); E. CRAVO AND A. C. FONSECA, *Few-Body Systems* **5**, 117 (1988).
21. G. H. RAWITSCHER AND E. S. HIRSCHORN, *J. Comput. Phys.* **68**, 104 (1987).
22. M. ABRAMOWITZ AND I. STEGUN (Eds.), *Handbook of Mathematical Functions* (Dover, New York, 1965).
23. S. KLARSFELD AND A. MARQUET, *Phys. Lett. A* **73**, 100 (1979); J. T. BROAD, *Phys. Rev. A* **31**, 1494 (1985); Z. PAPP, *Phys. Rev. C* **38**, 2457 (1988); H. MARXER, S. ALSTON, AND J BRIGGS, *Z. Phys. D* **8**, 177 (1988).
24. Y. HAHN, *Phys. Rev. A* **26**, 808 (1982); S. ADHIKARI AND L. TOMIO, *Phys. Rev. C* **36**, 1275 (1987); Y. SUN, D. J. KOURI, D. G. TRUHLAR, AND D. W. SCHWENKE, *Phys. Rev. A* **41**, 4857 (1990).
25. G. H. RAWITSCHER, *Phys. Rev. C* **39**, 440 (1989).